

---

# Noninvasive Oxygen Partial Pressure Measurement of Human Body Fluids In Vivo Using Magnetic Resonance Imaging<sup>1</sup>

Greg Zaharchuk, PhD, MD, Reed F. Busse, PhD, Guy Rosenthal, MD, Geoffery T. Manley, MD, PhD  
Orit A. Glenn, MD, William P. Dillon, MD

---

**Rationale and Objectives.** The oxygen partial pressure ( $pO_2$ ) of human body fluids reflects the oxygenation status of surrounding tissues. All existing fluid  $pO_2$  measurements are invasive, requiring either microelectrode/optode placement or fluid removal. The purpose of this study is to develop a noninvasive magnetic resonance imaging method to measure the  $pO_2$  of human body fluids.

**Materials and Methods.** We developed an imaging paradigm that exploits the paramagnetism of molecular oxygen to create quantitative images of fluid oxygenation. A single-shot fast spin echo pulse sequence was modified to minimize artifacts from motion, fluid flow, and partial volume. Longitudinal relaxation rate ( $R1 = 1/T1$ ) was measured with a time-efficient nonequilibrium saturation recovery method and correlated with  $pO_2$  measured in phantoms.

**Results.**  $pO_2$  images of human and fetal cerebrospinal fluid, bladder urine, and vitreous humor are presented and quantitative oxygenation levels are compared with prior literature estimates, where available. Significant  $pO_2$  increases are shown in cerebrospinal fluid and vitreous following 100% oxygen inhalation. Potential errors due to temperature, fluid flow, and partial volume are discussed.

**Conclusions.** Noninvasive measurements of human body fluid  $pO_2$  in vivo are presented, which yield reasonable values based on prior literature estimates. This rapid imaging-based measurement of fluid oxygenation may provide insight into normal physiology as well as changes due to disease or during treatment.

**Key Words.** Magnetic resonance imaging; oxygen; quantitation; T1; physiology.

© AUR, 2006

---

The oxygen partial pressure ( $pO_2$ ) of low-protein body fluids, such as urine, vitreous humor, and cerebrospinal fluid (CSF), is of physiologic interest, as such measurements may yield information about surrounding tissue oxygen levels (1–4). Current  $pO_2$  measurements require either fluid removal [and are susceptible to errors caused

by contamination from room air during fluid removal and analysis (5–7)] or the placement of invasive microelectrodes or optodes (4, 8–12). A truly noninvasive imaging-based method would enable body fluid oxygenation measurements under normal physiologic conditions or in the setting of disease (13). Another possibility is the opportunity to measure fetal fluid oxygenation, which may give unique insight into fetal well-being in utero (14). Such a method may also find use in nonmedical settings in which a nondestructive and noninvasive imaging-based oxygen measurement is desirable, such as cell viability assays (12) or for nondestructive analysis of beverage oxygenation (15).

---

**Acad Radiol** 2006; 13:1016–1024

<sup>1</sup> From the University of California, San Francisco, 505 Parnassus Avenue, San Francisco, California 94143-0628. Received March 29, 2006; accepted April 30, 2006. Address correspondence to G.Z. e-mail: Greg.Zaharchuk@radiology.ucsf.edu

© AUR, 2006

doi:10.1016/j.acra.2006.04.016

Evidence exists that oxygen monitoring of human body fluid collections is valuable. Invasive human studies show that lower CSF  $pO_2$  is associated with brain injury (10, 16). In animals, lumbar CSF  $pO_2$  rapidly decreases during transient spinal cord ischemia (4). Renal pelvic and bladder urine  $pO_2$  decreases during septic shock (17) and increases following administration of renal protective agents (18). Vitreous oxygenation changes following vitrectomy have been implicated in the development of nuclear sclerotic cataracts (19). Other work suggests that abnormalities in subretinal vitreous oxygenation during oxygen challenge are a potential early predictor of diabetic retinopathy (20).

Molecular oxygen ( $O_2$ ) has two unpaired electrons and is therefore paramagnetic. As for any low concentration paramagnetic solute, the water proton longitudinal relaxation rate  $R1$  ( $= 1/T1$ ) increases linearly with oxygen concentration (15, 21, 22).  $O_2$  is far more effective at causing  $R1$  changes than are equimolar amounts of protein, and previous authors have concluded that the proton NMR properties of many low-protein body fluids ( $<2$  g/L) are inseparable from water at the same temperature (23). A recent NMR-based study has used such a method to qualitatively estimate the rates of oxygen outgassing for commercially available hyperoxygenated beverage products, both in the bottle and in the human mouth and stomach (15, 24). More recently, these principles have been applied to measure quantitative CSF  $pO_2$ , using a time-consuming, spatially limited three-dimensional inversion recovery method (25).

This report outlines development of an MRI-based methodology to measure fluid oxygenation of low-protein human body fluids. A standard single-shot fast spin-echo (SSFSE) pulse sequence has been modified to minimize imaging artifacts and quantification errors caused by fluid flow and partial volume of surrounding tissue structures.  $R1$  is measured using a time-efficient, nonequilibrium saturation recovery approach, allowing  $pO_2$  maps to be acquired in several minutes. We have applied this method to measure  $pO_2$  noninvasively in cerebral and lumbar CSF, vitreous humor, and bladder urine of normal young adults. We demonstrate oxygenation changes in CSF and vitreous following supplemental oxygen inspiration. Finally, we present an example of the method for measuring oxygen content of fetal CSF and vitreous in utero.

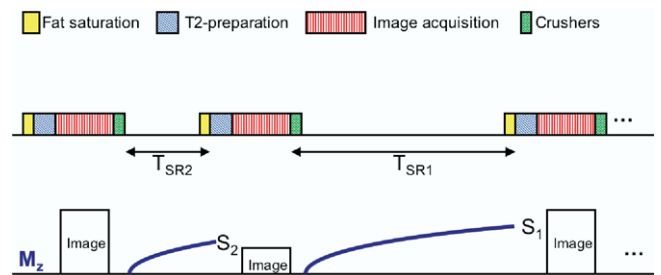


**Figure 1.** Schematic diagram of the SSFSE sequence and saturation recovery approach for  $pO_2$  imaging. Each imaging module consists of four parts: (i) fat saturation, which does not affect water spins; (ii) nonselective T2-preparation pulse cluster (27); (iii) SSFSE readout; and (iv) crusher gradients to destroy any remaining transverse magnetization. Note that the best representation of the time for longitudinal magnetization recovery ( $T_{SR1}$  and  $T_{SR2}$ ) is from the end of the FSE readout to the start of the T2-preparation cluster (26). In blue is a schematic of the longitudinal magnetization ( $M_z$ ) recovery. The ratio of the signal intensity in any voxel ( $S_1/S_2$ ) is solely a function of  $R1$  and can be determined using the iterative method described in Appendix A.

## MATERIALS AND METHODS

### Acquisition Method

A modified SSFSE pulse sequence was used to acquire a pair of images in succession at each location (Fig. 1). If longitudinal magnetization is completely recovered prior to the first acquisition ( $S_1$ ), saturated by the long train of refocusing pulses, and only partially recovered prior to the second acquisition ( $S_2$ ), then variation in signal intensity of the two acquisitions will be due only to longitudinal relaxivity ( $R1$ ). It should be noted that the appropriate recovery time for SSFSE images is from the end of the image readout period to the subsequent excitation (26). The ratio of  $S_1$  and  $S_2$  (as well as the saturation recovery times,  $T_{SR1}$  and  $T_{SR2}$ , of the two acquisitions) is used to calculate the  $R1$  of fluid on a voxel-by-voxel basis, as described in Appendix A. Variations in other MR parameters, such as proton density or  $T2$ , do not affect the  $S1/S2$  ratio or the  $R1$  value.

Fluid  $R1$  measurement is complicated by two factors: (i) partial volume in voxels containing both fluid and soft tissue and (ii) inflow of fluid with fresh spins after the initial saturation. To address the first, a long effective TE or a T2 preparatory (27) segment can be used prior to excitation to suppress nonfluid signal. To address the latter, nonselective T2 preparation and refocusing pulses are used during image acquisition; thus fluid, stationary or flowing, is equally saturated.

## Phantom Studies

Distilled water phantoms were prepared by bubbling mixtures of nitrogen ( $N_2$ ) and  $O_2$  gas to achieve a range of oxygenation, and direct  $pO_2$  measurement was performed using a polarographic electrode (Licox; GMS, Kiel-Mielkendorf, Germany). Glass volumetric flasks (10 ml) were submerged during the measurement and stoppered with ground-glass stoppers. Care was taken to exclude gas bubbles from the flasks. Phantoms with  $pO_2$  ranging from 7 to 276 mm Hg were placed into a water bath maintained at 37 °C within a 1.5-T MR scanner (Signa; GE Healthcare, Milwaukee, WI). Higher  $pO_2$  levels were not used because of the potential for bubble formation, which would change the dissolved oxygen concentration in an unpredictable fashion (15). Images were acquired using the following parameters:  $T_{SR1} = 10$  seconds,  $T_{SR2} = 3$  seconds,  $TE = 200$  milliseconds, field of view (FOV) = 20 cm, matrix  $320 \times 256$ , slice thickness = 8 mm, receiver bandwidth = 31.25 kHz, and echo train length = 136. R1 was determined by the iterative method described in Appendix A, using five iterations.

The effect of protein on the  $pO_2$  measurement was assessed by imaging a range of different concentrations of bovine serum albumin (BSA) (Sigma-Aldrich, St. Louis, MO) from 0 to 5 g/L in normal saline (0.9% NaCl). The samples were at equilibrium with room air, and measured within a water bath maintained at either room temperature (21 °C) or body temperature (37 °C). R1 measurements were performed using the same parameters as above.

## Human Studies

Our hospital's institutional review board approved the following study (total  $n = 17$ , 10 men and 7 women, mean age  $32 \pm 5$  years, age range 22–38 years). Not all subjects had all body fluid regions imaged; cerebral CSF and vitreous were imaged in 11 subjects (9 men and 2 women), bladder urine in 13 subjects (8 men and 5 women); and lumbar CSF in 9 subjects (7 men and 2 women). Prior informed consent was obtained. Images were acquired during room air breathing. In one subject (35-year-old man), cerebral CSF and vitreous images were acquired before and after 20 minutes of 100%  $O_2$  supplied by nonrebreather facemask (model 1060; Hudson RCI, Temecula, CA). In one 25-year-old pregnant woman, images were acquired of the maternal bladder and fetal fluids (CSF, vitreous) of her 30-week fetus; the scan was obtained to evaluate probable inferior vermian agenesis noted on prior ultrasound. The anatomical MRI confirmed this finding, and additionally noted left cerebel-

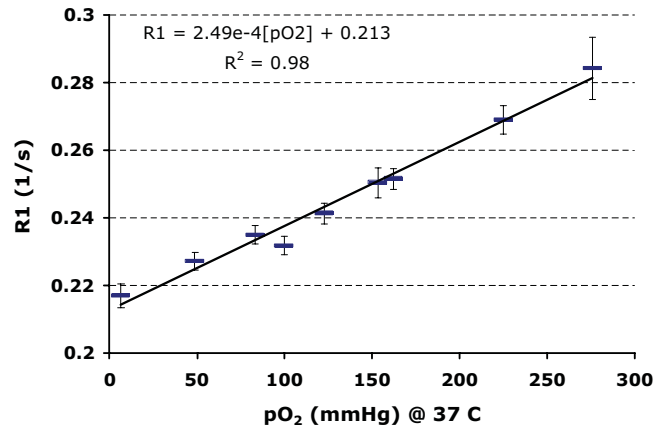


**Figure 2.** Plot of R1 ( $= 1/T_1$ , second $^{-1}$ ) for distilled water at body temperature (37 °C) and 1.5 T. Error bars show  $\pm 1$  standard deviation of the mean for 12 repeated measurements. The slope ( $\partial R_1/\partial pO_2$ ) and intercept [ $R_1(pO_2 = 0)$ ] were used to calibrate the human body fluid measurements.

lar hemisphere hypoplasia. The baby was born at term and was clinically normal in the newborn period.

The imaging sequence used for the human studies was the same as for the phantom study, with the exception of changes in FOV (24–35 cm; the minimum size was chosen that included the structures of interest), matrix ( $256 \times 256$ ), and slice thickness (5 mm for CSF and vitreous, 10 mm for bladder urine). Signal averaging of between 3 and 10 nex was used, resulting in a total imaging time of 45–150 seconds. To minimize partial volume errors, heavy T2-weighting was applied, either by using a TE of 750 milliseconds or using a 700-millisecond nonselective T2-preparatory segment (27) followed by image acquisition with a short (60 milliseconds) TE. These values were chosen based on simulations of partial volume errors (Appendix B). Conservative regions of interest were drawn manually for bladder urine and vitreous images. For CSF, thresholding of the images was performed based on signal intensity at a level expected to incur less than a 5 mm Hg error in  $pO_2$  due to partial volume effect.

## RESULTS

Figure 2 plots body-temperature distilled water R1 versus  $pO_2$  measured with a polarographic electrode, demonstrating a highly correlated linear slope. R1 of deoxygenated water was measured to be 0.213 second $^{-1}$ , 95% confidence range 0.208–0.217 second $^{-1}$ , corresponding to a T1 of 4.69 seconds (95% confidence range 4.61–4.81

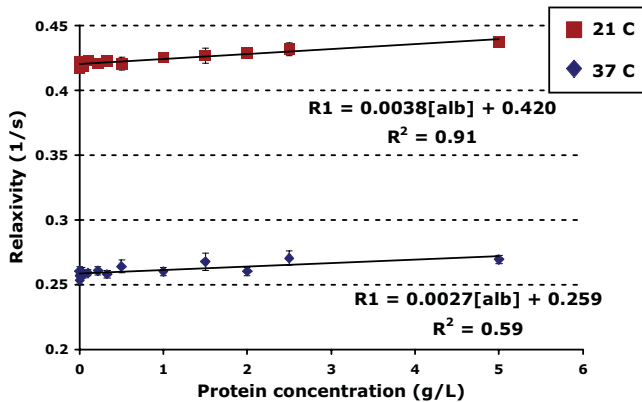


**Figure 3.** R1 versus protein concentration (BSA) of normal saline (0.9% NaCl) at both room and body temperature. The fluids were in equilibrium with room air. The R1 increase due to protein content at body temperature corresponds to an overestimation in  $pO_2$  of 11 mm Hg/(g/L protein), 95% confidence range 5–16 mm Hg/(g/L protein). The findings at room temperature compare well with those measured by previous investigators (33, 35). Error bars represent  $\pm 1$  SD of 12 repeated measurements.

seconds). The proportionality constant linking changes in R1 with changes in oxygen content ( $\partial R1/\partial pO_2$ ) was calculated to be  $2.49 \times 10^{-4}$  second $^{-1}$ /mm Hg, 95% confidence interval  $2.19$ – $2.78 \times 10^{-4}$  second $^{-1}$ /mm Hg.

Figure 3 shows the dependence of R1 on bovine serum albumin concentration. There is a linear increase in R1 due to protein, with an estimate of  $2.7 \times 10^{-3}$  second $^{-1}$ /(g/L), 95% confidence range  $1.3$ – $4.0 \times 10^{-3}$  second $^{-1}$ /(g/L) at 37 °C. This corresponds to an overestimation of  $pO_2$  by 11 mm Hg for every additional g/L of protein, with 95% confidence range 5–16 mm Hg/(g/L).

Typical R1 ( $pO_2$ ) maps of adult human CSF, vitreous, and bladder urine are shown as Figure 4. There is variation in CSF oxygenation in different parts of the brain, with highest oxygen concentrations overlying the cortical surfaces, and lower concentrations within the ventricular system. Vitreous and bladder urine images generally demonstrate relatively homogenous oxygenation, as might be expected in such well-mixed systems. The typical standard deviation of voxels measured centrally on the vitreous or bladder  $pO_2$  maps was on the order of 10–15% of the mean; this is purely determined by voxel size and imaging time, which may be traded off for one another. Table 1 presents the mean and standard deviation of  $pO_2$  measurements in different fluid compartments for all of the subjects along with best estimates from limited previous literature.

Figure 5 is a  $pO_2$  map of the pelvis in a pregnant 25-year-old woman, contrasting the relatively low  $pO_2$  of the

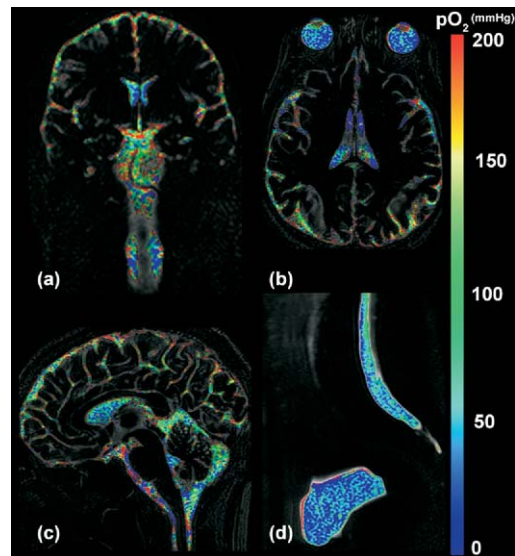


**Figure 4.** Representative  $pO_2$  images of CSF around the brain (a–c), the vitreous humor of the eye (b), the lumbar CSF (d), and bladder urine (d) in young adult subjects breathing room air. Differences between CSF  $pO_2$  surrounding different brain regions are evident. Vitreous and urinary oxygenation appears more homogenous. The color  $pO_2$  scale ranges from 0 to 200 mm Hg.

maternal bladder ( $62 \pm 18$  mm Hg) with the higher  $pO_2$  of the CSF of her 30-week fetus ( $124 \pm 90$  mm Hg). The fetal vitreous  $pO_2$  was  $66 \pm 53$  mm Hg. Figure 6 demonstrates the effect of 20 minutes of 100% oxygen inhalation on CSF and vitreous  $pO_2$  in a 35-year-old man. CSF  $pO_2$  increased from  $124 \pm 55$  mm Hg to  $228 \pm 18$  mm Hg in the cerebral sulci, while remaining unchanged in the lateral or fourth ventricles. Vitreous  $pO_2$  also increased from  $73 \pm 42$  mm Hg to  $93 \pm 22$  mm Hg.

## DISCUSSION

R1 changes in water attributable to paramagnetic molecular oxygen were first recognized by Bloch in the earliest NMR experiments (28). Subsequent investigators demonstrated the linear relationship between R1 and oxygen concentration predicted by theory (21, 22, 25). Using R1-based imaging methods to glean information regarding  $pO_2$  of human body fluids in vivo is a relatively new development (3, 24, 25). This may be due to several reasons: (i) the concept that  $O_2$  causes relatively large R1 changes compared with those due to natural variation in protein or macromolecular concentrations found in many body fluids (23); (ii) the difficulties in removing the effects of partial volume and fluid flow; and (iii) the inher-

**Table 1**  
**Comparison of MRI-Based Noninvasive pO<sub>2</sub> Measurement With Literature Values**

Region (n)	R1 (second <sup>-1</sup> )	pO <sub>2</sub> (mm Hg)	Literature "Best Estimates"	References
Cerebrospinal fluid				
Lateral ventricles (11)	0.226 ± 0.004	52 ± 14	30–74*†	7, 8, 11
Cisterna magna (11)	0.228 ± 0.007	62 ± 29	31–74†	1, 16
Cortical sulcal (11)	0.247 ± 0.011	138 ± 46	‡	‡
Lumbar subarachnoid (9)	0.230 ± 0.005	69 ± 22	40–57†	16, 39, 40
Vitreous (11)	0.228 ± 0.009	63 ± 34	9–20†	19, 43
Bladder urine (13)	0.228 ± 0.004	63 ± 16	25–80	17, 18, 38

MRI-based pO<sub>2</sub> measurement of human body fluids compared with prior invasive measurements. "Best estimates" are from prior reports in either normal animals\* or sick humans†, as only bladder urine pO<sub>2</sub> has been measured in normal humans.

‡No measurements in animals or humans. Findings are in reasonable concordance, except for vitreous oxygenation; possible reasons for this are discussed in the text.

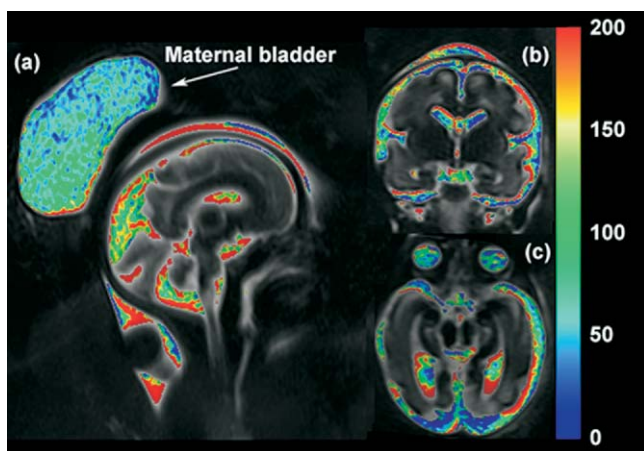


**Figure 5.** pO<sub>2</sub> images of a 25-year-old woman showing the maternal bladder, as well as the CSF and vitreous in a 30-week fetus in utero. The fetus is facing the viewer's right on the sagittal image (a). There is a striking difference in pO<sub>2</sub> between the maternal bladder urine (62 ± 18 mm Hg) and the fetal CSF (124 ± 90 mm Hg) (all CSF spaces included lateral ventricles, cortical sulci, and basilar cisterna). The fetal vitreous humor pO<sub>2</sub> was 66 ± 53 mm Hg. To our knowledge, these are the first measurements of fetal fluid oxygenation.

ent challenges surrounding measurement of long T1 substances, which can be time-consuming unless single-shot methods are used. No other paramagnetic substances are commonly found in most body fluid collections in significant concentrations; their presence in an abnormal state (such as transferrin in iron storage disorders or deoxyhemoglobin in the setting of hematuria) would be evident based on decreased T2 values, which are much more strongly affected by such large molecules than is T1.

The current SSFSE sequence (Fig. 1) has been purposefully modified to minimize artifacts due to fluid flow and partial volume, which can cause significant errors

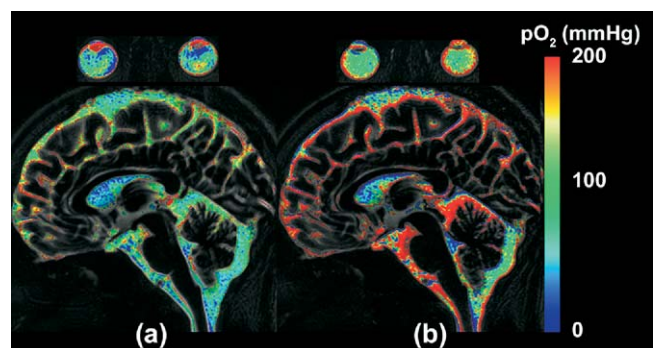


**Figure 6.** CSF and vitreous images (a) before and (b) following 20 minutes of 100% O<sub>2</sub> inhalation in a 35-year-old man. Images of the globes obtained from separate axial images are presented above the sagittal images of the brain CSF. Cortical sulcal CSF pO<sub>2</sub> increases from 124 ± 55 mm Hg to 228 ± 18 mm Hg, while no change is seen in the lateral or fourth ventricles. This pattern is consistent with "oxygen artifact" noted on FLAIR images. Smaller vitreous pO<sub>2</sub> increases were observed (from 73 ± 42 mm Hg to 93 ± 22 mm Hg).

when measuring R1. Most clinical SSFSE sequences use slice selective excitation and refocusing and are well known to demonstrate artifacts due to fluid flow in high flow regions, such as in CSF near the foramina of Monro and in the bladder due to ureteral jets (29, 30). The current method uses nonselective refocusing pulses during readout, which make the sequence less sensitive to flow during readout. If ultralong TE (750 milliseconds) or T2 preparation (27) followed by short TE (60 milliseconds) is used, the signal from surrounding short-T2 soft tissues is almost completely relaxed and does not affect the measurement. Also, because water has such a long T2 (>2000 milliseconds), there is minimal blurring even with readout times on the order of 1 second or longer, allowing for high spatial resolution imaging. In-plane mo-

tion can still cause signal loss due to intravoxel phase dispersion, but these errors are relatively small because the gradients used for refocusing the spin echoes have been minimized and the use of T2 preparation allows early sampling of magnetization before significant phase errors occur.

One potential error not addressed by these modifications is the change of R1 due to fluid temperature. Based on our phantom studies, we found a potential error  $\pm 19$  mm Hg for physiologic temperature fluctuations of  $\pm 1$  °C. While this sets a lower bound on the accuracy of the measurement, if the temperature is known [for example, estimated from oral or rectal measurement or using an MR-based temperature measurement (31)], pO<sub>2</sub> could be corrected by calculating a new baseline value for deoxygenated water. The proportionality constant ( $\partial R1/\partial pO_2$ ) is unlikely to change significantly for temperatures within physiologic range.

The phantom study of distilled body-temperature water with known dissolved oxygen concentrations again confirms a linear relationship between R1 and pO<sub>2</sub> in the physiologic range (Fig. 2). The measurement of deoxygenated body-temperature water of 0.213 second<sup>-1</sup> is near that estimated by Hopkins et al. (0.22 second<sup>-1</sup>) and in line with previous measurements using a time-consuming three-dimensional inversion recovery method (0.226 second<sup>-1</sup>) (23, 25). The measured ratio of R1 to pO<sub>2</sub> changes ( $\partial R1/\partial pO_2$ ) is also similar to prior measurements (25) and falls between values observed at higher and lower magnetic field strengths (3, 32). Distilled water was used in this experiment for convenience, as previous studies have shown no differences in these parameters between distilled water, normal saline, or water with up to 2 g/L dissolved protein (25, 33, 34). Figure 3 demonstrates this weak dependence of R1 on protein levels. The room-temperature measurements are similar to those obtained by other investigators (33, 35); the body-temperature measurements suggest that any overestimation of pO<sub>2</sub> due to relaxivity from proteins is on the order of 5–16 mm Hg/(g/L of protein) (for reference, normal CSF protein is 0.3 g/L). It should be noted that these studies were performed with a single, large, negatively charged protein (BSA), and the results may be different for other proteins.

Many invasive studies document the relationship and importance of pO<sub>2</sub> changes in specific disease states and for patient outcomes (4, 8, 10, 16, 18, 19), but difficulties associated with microelectrode placement and the exclusion of room air oxygen from fluid samples have limited widespread use of pO<sub>2</sub> monitoring. A noninvasive tech-

nique such as MRI obviates problems associated with room air contamination and invasive catheter placement, allowing wider application of pO<sub>2</sub> monitoring, including the study of normal human and fetal physiology.

pO<sub>2</sub> maps of adult human body fluid collections are shown in Figure 4. Vitreous and bladder pO<sub>2</sub> images appear relatively homogeneous, while CSF images demonstrate regional differences between compartments, with lower CSF pO<sub>2</sub> in the lateral ventricles compared with the cerebral cortical sulci and the basilar cisterns. Following inhalation of 100% oxygen, significant increases in CSF pO<sub>2</sub> within the vitreous and the CSF in the cortical sulci, basilar cisterna, and cisterna magna are noted (Fig. 6). No changes were seen in the lateral or fourth ventricles. Of interest, this pattern is identical to the “artifact” noted on fluid-attenuated inversion recovery (FLAIR) sequences in the presence of supplemental oxygen, further confirmation that these findings are related to the presence of dissolved oxygen within the CSF (33, 36). Our initial images of the maternal pelvis demonstrate oxygenation differences between fluid in the maternal bladder and the fetal CSF (Fig. 5). To our knowledge, this is the first measurement of fetal fluid oxygenation made with any method. No measurements of amniotic fluid pO<sub>2</sub> were made, given that the protein content of the amniotic fluid can be quite high (up to 8 g/L) and varies with gestation (37).

Comparing the current measurements to prior literature values is difficult, as only bladder urine pO<sub>2</sub> has been measured in normal humans using invasive techniques. Studies of urinary oxygenation have yielded a wide range (25–80 mm Hg), which is apparently dependent on hydration and diet (2, 17, 18, 38). Various studies report CSF values between 31 and 74 mm Hg in hospitalized patients (8, 10, 16, 39, 40). Additionally, the levels reported in the current study are quite similar to those measured in the CSF surrounding the brain using a three-dimensional inversion recovery MRI method in normal subjects (25). Thus, we believe that the measurements from the current study are compatible with previous measurements of bladder urine and cerebral CSF. The current measurement of  $63 \pm 24$  mm Hg for vitreous pO<sub>2</sub> is significantly higher than that measured invasively in previtrectomy patients and in animals (between 9 and 20 mm Hg) (19, 41). One possible reason may be the difference between the current study of young normal subjects and the older patients who were previtrectomy for significant ocular pathologies. Another explanation is that the current measurement may be in error due to blinking or other eye movements (42). Finally, T1 shortening in excess of that

expected based on concentration due to proteoglycans and collagen within the vitreous gel may be present, and further investigations on this possibility are ongoing. Fetal  $pO_2$  measurements are roughly the same as in adults, with a similar difference between the fetal vitreous and cortical CSF levels. The background noise of the measurements is higher than for adults, due to the small size of the fetal structures and the relatively low sensitivity of a body receive coil, although this could be improved by longer imaging times or dedicated surface coils.

While this report discusses a specific medical application, it is possible that this method may find use in other situations in which a noninvasive, nondestructive measurement of oxygen content is of interest. One application is quality control of oxygen content of commercially produced hyperoxygenated beverages (15). Another might be application to closed biological systems, particularly for experiments that monitor the effects of controlled oxygen environments on cell growth and viability (12). Certainly, one could envision monitoring the decrease in molecular oxygen within a fluid supernatant surrounding viable aerobic cells during oxidative metabolism. The current imaging-based method might lend itself to multiwell batch processing schemes. In the medical arena, we suspect that this method will permit more widespread evaluation of oxygenation changes that occur during normal human physiology, in the setting of disease, or during treatment.

## REFERENCES

- Jarnum S, Lorenzen I, Skinhøj E. Cisternal fluid oxygen tension in man. *Neurology* 1964; 14:703-707.
- Rennie DW, Reeves RB, Pappenheimer JR. Oxygen pressure in urine and its relation to intrarenal blood flow. *Am J Physiol* 1958; 195:120-132.
- Berkowitz BA. Adult and newborn rat inner retinal oxygenation during carbogen and 100% oxygen breathing. Comparison using magnetic resonance imaging delta  $pO_2$  mapping. *Invest Ophthalmol Vis Sci* 1996; 37:2089-2098.
- Lips J, de Haan P, Bouma GJ, et al. Continuous monitoring of cerebrospinal fluid oxygen tension in relation to motor evoked potentials during spinal cord ischemia in pigs. *Anesthesiology* 2005; 102:340-345.
- Grant R, Condon B, Moyns S, et al. Temporal physiochemical changes during in vitro relaxation time measurements: The cerebrospinal fluid. *Magn Reson Med* 1988; 6:397-402.
- Bejar R, Giussi G, Casacuberta C, et al. The actual value of  $pO_2$  in human amniotic fluid. *Eur J Obstet Gynecol* 1971; 6:189-193.
- Venkatesh B, Boots RJ. Carbon dioxide and oxygen partial pressure measurements in the cerebrospinal fluid in a conventional blood gas analyzer: Analysis of bias and precision. *J Neurol Sci* 1997; 147:5-8.
- Bloor BM, Fricker J, Hellinger F, et al. A study of cerebrospinal fluid oxygen tension. *Arch Neurol* 1961; 4:37-46.
- Vasicka A, Hutchinson HT. Oxygen tension in amniotic fluid and fetal distress. *Am J Obstet Gynecol* 1964; 88:530-540.
- Venkatesh B, Boots RJ, Tomlinson E, et al. The continuous measurement of cerebrospinal fluid gas tensions in critically ill neurosurgical patients: A prospective observational study. *Intensive Care Med* 1999; 25:599-605.
- Maas AIR, Fleckenstein W, de Jong DA, et al. Monitoring cerebral oxygenation: Experimental studies and preliminary clinical results of continuous monitoring of cerebrospinal fluid and brain tissue oxygen tension. *Acta Neurochir Suppl* 1993; 59:50-57.
- Hynes J, Floyd S, Soini AE, et al. Fluorescence-based cell viability screening assays using water-soluble oxygen probes. *J Biomol Screen* 2003; 8:264-272.
- Grucker D. Oxymetry by magnetic resonance: Applications to animal biology and medicine. *Progr NMR Spectrosc* 2000; 36:241-270.
- Johnell HE, Nilsson BA, Tammivaara-Hilty R. Oxygen tension, carbon dioxide tension and pH in amniotic fluid and maternal arterial blood during induced maternal hyperoxia and hypoxia. *Acta Obstet Gynecol Scand* 1971; 50:207-214.
- Nestle N, Baumann T, Neissner R. Oxygen determination in oxygen-superaturated drinking waters by NMR relaxometry. *Water Res* 2003; 37:3361-3366.
- Rossanda M, Gordon E. The oxygen tension of cerebrospinal fluid in patients with brain lesions. *Acta Anaesth Scand* 1970; 14:173-181.
- Leonhardt KO, Landes RR. Oxygen tension of the urine and renal structures. *New Engl J Med* 1963; 269:115-121.
- Morelli A, Rocco M, Conti G, et al. Monitoring renal oxygen supply in critically-ill patients using urinary oxygen tension. *Anesth Analg* 2003; 97:1764-1768.
- Holekamp NM, Shui YB, Beebe DC. Vitrectomy surgery increases oxygen exposure to the lens: A possible mechanism for nuclear cataract formation. *Am J Ophthalmol* 2005; 139:302-310.
- Ito Y, Berkowitz BA. MR studies of retinal oxygenation. *Vision Res* 2001; 41:1307-1311.
- Chiarotti G, Cristiani G, Giulotto L. Proton relaxation in pure liquids and in liquids containing paramagnetic gases in solution. *Nuovo Cimento* 1955; 1:863-872.
- Mirhej ME. Proton spin relaxation by paramagnetic molecular oxygen. *Can J Chem* 1965; 43:1130-1138.
- Hopkins AL, Yeung HN, Bratton CB. Multiple field strength in vivo T1 and T2 for cerebrospinal fluid protons. *Magn Reson Med* 1986; 3:303-311.
- Nestle N, Wunderlich A, Nussle-Kugele K. In vivo observation of oxygen-supersaturated water in the human mouth and stomach. *Magn Reson Imaging* 2004; 22:551-556.
- Zaharchuk G, Martin AJ, Rosenthal G, et al. Measurement of cerebrospinal fluid oxygen partial pressure in humans with MRI. *Magn Reson Med* 2005; 54:113-121.
- Lee JN, Riederer SJ. A modified saturation-recovery approximation for multiple spin-echo pulse sequences. *Magn Reson Med* 1986; 3:132-134.
- Brittain JH, Hu BS, Wright GA, et al. Coronary angiography with magnetization-prepared T2 contrast. *Magn Reson Med* 1995; 33:689-696.
- Bloch F, Hansen WW, Packard M. The nuclear induction experiment. *Physiol Rev* 1946; 70:474-485.
- Tanaka N, Abe T, Kojima K, et al. Applicability and advantages of flow artifact-insensitive fluid-attenuated inversion-recovery MR sequences for imaging the posterior fossa. *AJNR Am J Neuroradiol* 2000; 21:1095-1098.
- Kallmes DF, Hui FK, Mugler JP 3rd. Suppression of cerebrospinal fluid and blood flow artifacts in FLAIR MR imaging with a single-slab three-dimensional pulse sequence: initial experience. *Radiology* 2001; 221:251-255.
- Corbett RJ, Laptok AR, Tollefsbol G, et al. Validation of a noninvasive method to measure brain temperature in vivo using  $^1H$  NMR spectroscopy. *J Neurochem* 1995; 64:1224-1230.
- Lai C-S, Stair SJ, Miziorko H, et al. Effect of oxygen and the lipid spin label TEMPO-laurate on fluorine-19 and proton relaxation rates of the perfluorochemical blood substitute, FC-43 emulsion. *J Magn Reson* 1984; 57:447-452.
- Anzai Y, Ishikawa M, Shaw DWW, et al. Paramagnetic effect of supplemental oxygen on CSF hyperintensity on fluid-attenuated inversion recovery MR images. *Am J Neuroradiol* 2004; 25:274-279.
- Castro ME, Boisvert DP, Treiber EO, et al. Effect of CSF albumin concentration on NMR relaxation properties. In *Proceedings of Society of Magnetic Resonance in Medicine*, New York, NY, 1984, p. 138.
- Yilmaz A, Ulak FS, Batun MS. Proton T1 and T2 relaxivities of serum proteins. *Magn Reson Imaging* 2004; 22:683-688.

36. Deliganis AV, Fisher DJ, Lam AM, et al. Cerebrospinal fluid signal intensity increase on FLAIR MR images in patients under general anesthesia: The role of supplemental O<sub>2</sub>. *Radiology* 2001; 218:152–156.
37. Dallaire L, Milunsky A. Amniotic fluid. In: Milunsky A (ed.) *Genetic Diseases and the Fetus: Diagnosis, Prevention, and Treatment*. Baltimore, MD: The Johns Hopkins University Press, 2004, p. 107.
38. Giannakopoulos X, Evangelou A, Kalfakakou V, et al. Human bladder urine oxygen content: Implications for urinary tract diseases. *Int Urol Nephrol* 1997; 29:393–401.
39. Dunkin RS, Bondurant S. The determinants of cerebrospinal fluid pO<sub>2</sub>. *Ann Intern Med* 1966; 64:71–80.
40. Gaenshirt V. Die Sauerstoffdruck im Liquor cerebrospinalis. *Wiener Medizinische Wochenschrift* 1966; 116:953–954.
41. Sakaue H, Akira N, Honda Y. Comparative study of vitreous oxygen tension in human and rabbit eyes. *Invest Ophthalmol Vis Sci* 1989; 30:1933–1937.
42. Berkowitz BA, McDonald C, Ito Y, et al. Measuring the human retinal oxygenation response to a hyperoxic challenge using MRI: Eliminating blinking artifacts and demonstrating proof of concept. *Magn Reson Med* 2001; 46:412–416.
43. Sakaue H, Tsukahara Y, Negi A, et al. Measurement of vitreous oxygen tension in human eyes. *Jpn J Ophthalmol* 1989; 33:199–203.

**APPENDIX A**

**Iterative R1 Measurement Using a Dual-Shot SSFSE Sequence**

If two SSFSE images are acquired in succession, with the magnetization fully recovered prior to the first acquisition (#1), saturated by a long train of refocusing pulses and postimage crusher gradients, then followed by a time period (T<sub>SR2</sub>), at which time the second acquisition (#2) occurs, the signal intensity of the two acquisitions are as follows:

$$S_1 = M_0 \exp(-TE/T_2) \tag{A1}$$

$$S_2 = M_0(1 - \exp(-T_{SR2}/T_1))\exp(-TE/T_2)$$

where M<sub>0</sub> is the initial longitudinal magnetization and TE is the echo time. These equations may be solved for T<sub>1</sub> analytically:

$$T_1 = \frac{-T_{SR2}}{\ln(1 - S_2/S_1)} \tag{A2}$$

Given the long T<sub>1</sub> of CSF (>4 seconds), it is time-consuming to wait >5 T<sub>1</sub> for complete relaxation back to equilibrium. Improved SNR per unit time can be achieved using a shorter period between successive acquisitions. In this case, incomplete recovery in the initial image will lead to T<sub>1</sub> underestimation; however, because this time (T<sub>SR1</sub>) is known, the effect of partial saturation on S<sub>1</sub> can be calculated and the T<sub>1</sub> estimate iteratively improved. A new estimate (T'<sub>1</sub>) is based on the previous iteration's estimate (T<sub>1</sub>) according to:

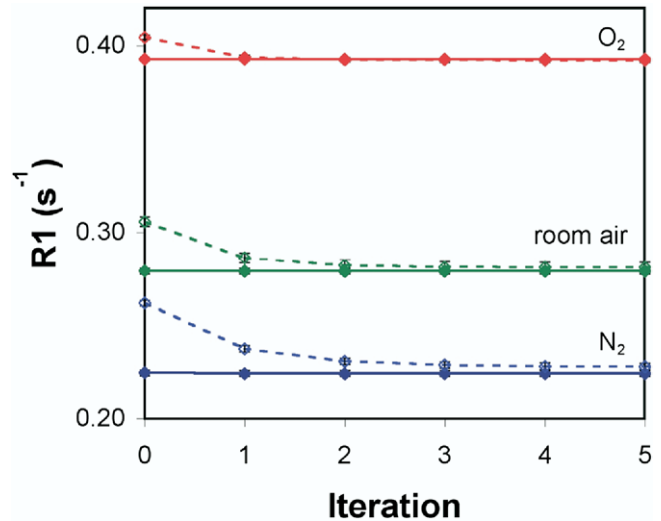


**Figure 7.** Demonstration of the efficacy of the iterative T<sub>1</sub> method. Measurements were made in distilled water at 37 °C following 5 minutes of bubbling of 100% N<sub>2</sub> gas, room air (21% O<sub>2</sub>, balance N<sub>2</sub>), or 100% O<sub>2</sub> gas. Initial estimates overestimate R<sub>1</sub> when the sample is not fully recovered, but the iterative refinement corrects this overestimation. In practice, five iterations were sufficient for convergence and were used for the measurements in this study.

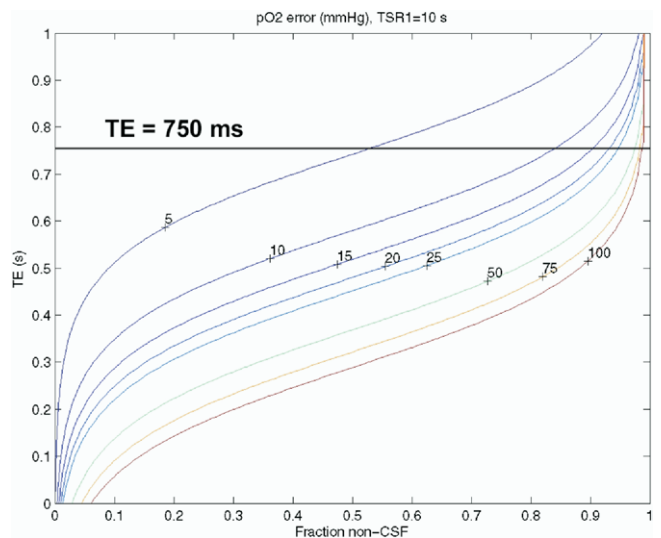


**Figure 8.** The effect of partial volume on fluid pO<sub>2</sub> measurements was simulated using a two-compartment model as a function of TE, assuming typical soft tissue parameters (T<sub>1f</sub> = 1 second, T<sub>2f</sub> = 0.1 second), fluid parameters (T<sub>1f</sub> = 4 seconds, T<sub>2f</sub> = 2 seconds), and the imaging parameters from the current study (T<sub>SR1</sub> = 10 seconds, T<sub>SR2</sub> = 3 seconds). pO<sub>2</sub> overestimation (in units of mm Hg) is shown for known nonfluid volume fraction and chosen TE. The black horizontal bar indicates the effective TE used in the current study, showing that less than 5 mm Hg error is expected for up to 50% inclusion of nonfluid material within a given voxel.

$$T_1' = \frac{-T_{SR2}}{\ln\left(1 - \frac{S_2}{S_1/(1 - \exp(-T_{SR1}/T_1))}\right)} \quad (\text{A3})$$

Figure 7 shows an example of the T1 estimation error due to short  $T_{SR1}$  and correction with the iterative method. In practice, we have found rapid convergence to the true T1 and chose to use five iterations for the measurements described in this report.

## APPENDIX B

### Effects of Partial Volume Contamination on $pO_2$ Measurement

Fluid T1 is much longer than that of surrounding soft tissue structures. Thus, inadvertent inclusion of this tissue leads to R1 overestimation. The error can be severe for even small amounts of partial volume (<5%), which may not be easily recognizable on MR images.

The transverse relaxation time (T2) of low-protein fluid is also quite long and suggests a solution based on ultralong effective TE. We performed two-compartment simulations to assess the  $pO_2$  error due to inadvertent inclusion of soft tissue (Fig. 8). These curves are based on reasonable assumptions for the relaxivity of the two compartments: fluid  $T1_f = 4$  seconds,  $T2_f = 2$  seconds; soft tissue  $T1_t = 1$  second,  $T2_t = 0.1$  second;  $T_{SR1}$  and  $T_{SR2}$  are the same as those used for the human  $pO_2$  mapping (10 and 3 seconds, respectively). These simulations suggest that the effect of partial volume on the  $pO_2$  measurement decreases significantly with increasing TE. In fact, for TE equal to or greater than 750 milliseconds, even 50% partial volume with surrounding tissue causes an overestimation of the  $pO_2$  level of less than 5 mm Hg. For such long TEs, the SNR loss is minimal for fluid due to its long T2; however, the signal from surrounding soft tissue structures is almost completely relaxed before image acquisition.